THE JOURNAL OF PHYSICAL CHEMISTRY B

ARTICLE

pubs.acs.org/JPCB

SRLS Analysis of ^{15}N Spin Relaxation from *E. coli* Ribonuclease HI: The Tensorial Perspective

Eva Meirovitch,*[,†] Yury E. Shapiro,[†] Mirco Zerbetto,[‡] and Antonino Polimeno[‡]

[†]The Mina and Everard Goodman Faculty of Life Sciences, Bar-Ilan University, Ramat-Gan 52900, Israel

[‡]Department of Chemistry, University of Padua, 35131 Padua, Italy

ABSTRACT: ^{15}N−H relaxation parameters from ribonuclease HI (RNase H), acquired in previous work at magnetic fields of 14.1 and 18.8 T, and at 300 K, are analyzed with the mode-coupling slowly relaxing local structure (SRLS) approach. In accordance with standard theoretical treatments of restricted motions, SRLS approaches N−H bond dynamics from a tensorial perspective. As shown previously, a physically adequate description of this phenomenon has to account for the asymmetry of the local spatial restrictions. So far, we used rhombic local ordering tensors; this is straightforward but computationally demanding. Here, we propose substantiating the asymmetry of the local spatial restrictions in terms of tilted axial local ordering ($\boldsymbol{S}$) and local diffusion ($\boldsymbol{D_2}$) tensors. Although less straightforward, this description provides physically sound structural and dynamic information and is efficient computationally. We find that the local order parameter, S_0^2, is on average 0.89 (0.84, and may be as small as 0.6) for the secondary structure elements (loops). The main local ordering axis deviates from the $C_{i-1}^{\alpha}-C_i^{\alpha}$ axis by less than 6°. At 300 K, $D_{2,\perp}$ is virtually the same as the global diffusion rate, $D_1 = 1.8 \times 10^7$ s^{-1}. The correlation time $1/6D_{2,\parallel}$ ranges from 3−125 (208−344) ps for the secondary structure elements (loops) and is on average 125 ps for the C-terminal segment. The main local diffusion axis deviates from the N−H bond by less than 2° (10°) for the secondary structure elements (loops). An effective data-fitting protocol, which leads in most cases to unambiguous results with limited uncertainty, has been devised. A physically sound and computationally effective methodology for analyzing ^{15}N relaxation in proteins, that provides a new picture of N−H bond structural dynamics in proteins, has been set forth.

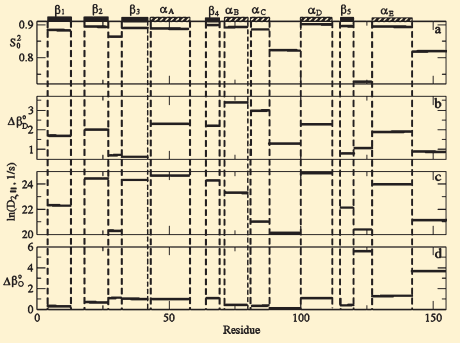

1. INTRODUCTION

Ribonuclease HI (RNase H, EC 3.1.26.4) is an endonuclease that hydrolyzes the RNA strand in RNA−DNA hybrid molecules.[1−4] *Escherichia coli* RNase H participates in DNA replication by defining the origin of replication in ColEl plasmids;[5−7] inhibiting replication from genomic sites other than oriC;[8,9] and removing RNA oligonucleotides from Okazaki fragments during lagging strand synthesis.[10] Retroviral reverse transcriptase (RT) contains a C-terminal RNase H domain that has been shown to be involved in at least three processes essential for reverse transcription.[11]

Escherichia coli RNase consists of a single polypeptide chain comprising 155 amino acid residues. The three-dimensional structure of this enzyme was determined by X-ray crystallography[12−14] and NMR.[15] RNase H is a α/β protein with five α-helices denoted α_A to α_E (residues 43 to 58, 71 to 80, 81 to 88, 100 to 112, and 127 to 142), and a five-stranded β-sheet, comprising the strands denoted β_1 to β_5 (residues 4 to 13, 18 to 27, 32 to 42, 64 to 69, and 115 to 120).[12] The polypeptide chain segment containing residues 90 to 99 has been termed the handle region,[12] while the overlapping region from residues 81 to 99 has been termed the basic protrusion.[14] The backbone structure of RNase H is illustrated in Figure 1.[17]

The secondary structure of the protein in solution agrees with its crystallographic counterpart.[18] Results obtained from model building[12,14,19] and NMR spectroscopy[19,20] are consistent with the presumed locations of the catalytic and binding sites. The loops between β_1 and β_2, α_C and α_D, and β_5 and α_E have been suggested to participate in substrate binding.

RNase H has been studied extensively with NMR spectroscopy.[11,15,17,21−27] Of particular interest to the present study are model-free (MF) analyses of autocorrelated relaxation parameters, ^{15}N T_1, T_2 and ^{15}N−{^{1}H} *NOE*,[11,17,26,27] and cross-correlated relaxation parameters, η_{xy} and η_z,[25] associated with backbone amide bonds. MF is a simple method valid in the limit where the local motion of the N−H bond and the global motion of the protein may be considered statistically independent (decoupled), and the tensorial properties are very simple. MF features analytical spectral densities (that underlie the expressions for the relaxation parameters) based on mathematical considerations.[28−30]

References 11, 17, and 25 describe careful MF analyses of good experimental data obtained from an RNase molecule considered spherically symmetric. Nevertheless, several significant inconsistencies emerged. For example, the temperature-dependence of the generalized MF order parameter, S, was used to calculate a characteristic temperature, T^*, for the motion of the backbone N−H

Received: September 11, 2011
Revised: November 29, 2011
Published: November 29, 2011

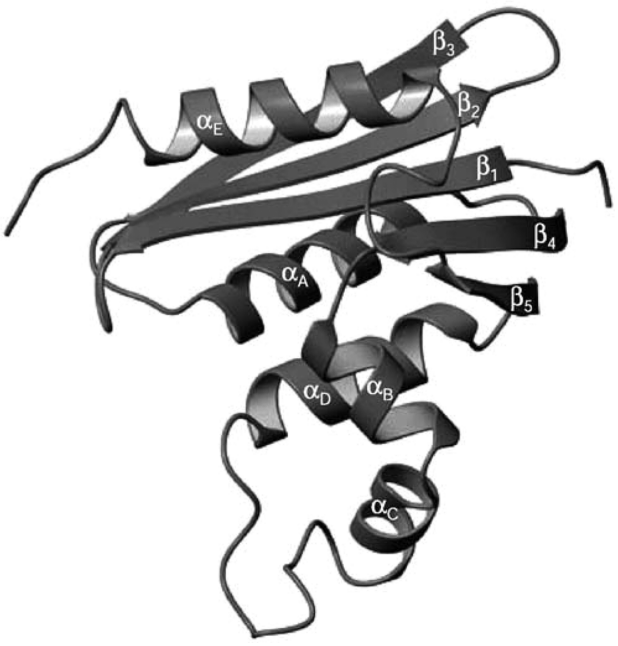

Figure 1. Structure of *E. coli* RNase H. This enzyme is a α/β protein with five a-helices, denoted α_A to α_E (residues 43−58, 71−80, 81−88, 100−112, and 127−142) and a five-stranded β-sheet, comprising the strands denoted β_1 to β_5 (residues 4−13, 18−27, 32−42, 64−69, and 115−120). The figure was drawn with the program MOLSCRIPT (ref 16) using the PDB coordinate file 1RNH (ref 12). Reprinted from ref 17. Copyright 1996 American Chemical Society.

bond vectors on the ps to ns time scale.[17] For that, a given form was assumed for the axial local ordering potential, with T^* related analytically to its coefficient. Using the latter, we calculated an S^2 value that is 14% smaller than the value determined with the MF analysis.[17]

^{15}N relaxation parameters of RNase H were also acquired at 14.1 and 18.8 T.[25] The purpose of that study was to investigate the variability of the ^{15}N chemical shift anisotropy (CSA) tensor. In addition to good statistics, the methodology used required that the N−H bonds employed in the analysis be free of slow local motional effects and conformational exchange contributions, R_{ex}. These requirements were fulfilled by the single-field data. However, we found that combined data acquired at two or three magnetic fields yield different results (this is a common problem in MF analyses; see, for example, ref 31). In particular, R_{ex} contributions, often associated with different residues at different magnetic fields, emerged for approximately 50% of the relevant N−H bonds.

Clearly, many of these R_{ex} terms are artificial. One can eliminate quite a few by accounting for an axial global diffusion tensor, $\boldsymbol{D_1}$, with $D_{1,\|}/D_{1,\perp} = 1.23$, determined with standard MF methods.[26] However, we show below with predictive calculations that such small deviation of $\boldsymbol{D_1}$ from spherical symmetry may be ignored. Hence, one has to search for effects other than $\boldsymbol{D_1}$ axiality having been absorbed by the artificial R_{ex} terms.

Inconsistencies of the kind described above arise when the model used is oversimplified or when data imperfection is substantial. If the latter factor is dominant, the inconsistencies will persist when an enhanced model is used. If model oversimplification is the dominant reason, the inconsistencies are expected to be reduced to a negligible level by a physical description that matches data sensitivity.

We developed in recent years the slowly relaxing local structure (SRLS) approach[32−34] for NMR spin relaxation analysis in proteins.[35−37] SRLS is a two-body (protein and probe) coupled-rotator model that (among others) describes the local motion and the local ordering in terms of second rank tensors. When a given description is oversimplified, it can be enhanced in a physically sound manner by lowering tensor symmetry and/or increasing geometric complexity. Enhanced descriptions require typically more extensive numerical calculations.

We determined previously the factors that are important for a physically adequate description of N−H bond dynamics in proteins. The asymmetry of the local spatial restrictions at the site of the motion of the N−H bond was found to be a key factor.[36−40] Independent methods, such as the 3D Gaussian axial fluctuations (GAF) model,[41,42] and molecular dynamics (MD) simulations,[43−45] led to a similar conclusion. The straightforward approach for representing this asymmetry is to allow for rhombic local ordering tensors.[36−38,40,46−53] However, the respective SRLS calculations are computationally demanding. Here, we represent the asymmetry of the local spatial restrictions in terms of tilted axial local ordering and local diffusion tensors. This description is less straightforward. However, it provides physically sound structural and dynamic information and is computationally efficient.

SRLS is the generalization of MF.[36,37,40] It yields the analytical MF spectral densities in limits of high tensor symmetry and simple geometric features by solving the appropriate Smoluchowski equations.[54,55] Rhombic local ordering and properly tilted tensor frames are outside the scope of MF. Because the MF spectral density is given by a fixed expression, so-called enhancements can only be made by redefining its features, notably the parameters that enter it, in terms of constructs with a vague physical meaning.[56] For example, the inherently axial order parameter,[54] already generalized in the spectral density of ref 28, has been redefined as a composite that also includes geometric factors and even rhombic components of the magnetic tensors.[56]

In this article, we present a systematic procedure based on physical parameters for analyzing ^{15}N relaxation data in proteins. We start with the MF limit[28] where the local ordering tensor, $\boldsymbol{S}$, is axial and collinear with the ^{15}N−^{1}H dipolar tensor whose principal axis points along the N−H bond. The dipolar tensor is also collinear with the ^{15}N CSA tensor (taken axial). The local diffusion tensor, $\boldsymbol{D_2}$, is approximated as isotropic (a restricted motion is in principle anisotropic).[57,58] The global diffusion tensor is taken as isotropic. This simple description is enhanced gradually. Only results that yield good statistics, ensure internal consistency, and agree with the structural context are accepted and used to obtain quantitative information. The final picture obtained in this manner is physically sound and commensurate with the sensitivity of the experimental data.

Problems of overfitting and force-fitting (or under-fitting), which are of particular concern when the spectral density is an intricate function and the number of free variables is relatively large, are also addressed. This is done within the scope of a fitting scheme where the starting values of the free variables are chosen based on physical considerations. In most cases, unambiguous results with limited uncertainties are obtained.

The tensorial perspective offered in this study provides quantitative information on the strength of the local ordering and the magnitudes of the local motional rates at every N−H site in the protein. It also provides geometric information given by the

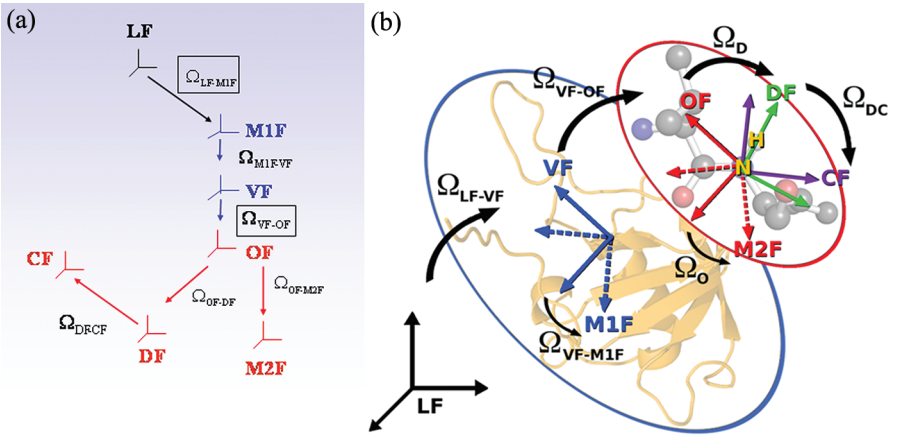

Figure 2. (a) LF is the space-fixed laboratory frame with its Z axis parallel to the external magnetic field. M1F is the principal axis system (PAS) of the global diffusion tensor, $\boldsymbol{D}_1$. VF is the local director. The M1F and VF frames are fixed in the protein (blue). The OF frame is the PAS of the local ordering tensor, $\boldsymbol{S}$. M2F is the PAS of the local diffusion tensor, $\boldsymbol{D}_2$. DF is the PAS of the magnetic $^{15}N-^{1}H$ dipolar tensor. CF is the PAS of the ^{15}N chemical shift anisotropy tensor. OF, M2F, DF, and CF are fixed in the probe (red). The Euler angles Ω_{M1F-VF}, Ω_{OF-M2F}, Ω_{OF-DF}, and Ω_{DF-CF} are time-independent. The time-dependent Euler angles (boxed), Ω_{LF-M1F}, are modulated by the global motion. The distributed Euler angles (boxed), Ω_{VF-OF}, are associated with the local ordering. (b) Pictorial presentation of the frames are shown in panel a, in the context of a typical protein structure. Note that in panel b the frames VF and M1F are separated. This corresponds to the general case in which the global diffusion tensor, $\boldsymbol{D}_1$, with PAS M1F, is nonspherically symmetric.

orientations of the local ordering and local diffusion tensors relative to the magnetic tensors.

2. THEORETICAL BACKGROUND

2.1. Slowly Relaxing Local Structure Approach. The full two-body Smoluchowski SRLS theory as applied to NMR spin relaxation in proteins is outlined in refs 35−37 and 40. A brief summary is given below. The SRLS frames are depicted in Figure 2a: they are illustrated pictorially in the context of a typical protein structure in Figure 2b.

For describing the local motion, we use a relative (probe versus protein) coordinate scheme. That is, the local ordering frame, OF, fixed in the probe, is distributed with respect to the local director frame, VF, fixed in the protein. VF is associated with the conformation for which the local ordering potential is at minimum. Each axial rotator when uncoupled is associated with three decay rates, $\tau_K^{-1} = 6D_\perp + K^2(D_\parallel - D_\perp)$, $K = 0, 1, 2$, where D stands for either D_1 or D_2.[33,34,36,37,40] In this study, we take $\boldsymbol{D}_1$ to be isotropic and allow $\boldsymbol{D}_2$ to be axially symmetric. The two rotators are coupled by the potential of mean torque (POMT), $U(\Omega_{VF-OF})$.[32,35] The diffusion equation for the coupled system is given by[36,37,40]

$$\frac{\partial}{\partial t}P(X,t) = -\hat{\Gamma}P(X,t) \tag{1}$$

where X is a set of coordinates completely describing the system. One has

$$X = (\Omega_{VF-OF}, \Omega_{LF-VF})$$
$$\hat{\Gamma} = \hat{\mathrm{J}}^{\mathrm{t}}(\Omega_{VF-OF})\boldsymbol{D}_2 P_{eq}\hat{\mathrm{J}}(\Omega_{VF-OF})P_{eq}^{-1} + [\hat{\mathrm{J}}(\Omega_{VF-OF}) - \hat{\mathrm{J}}(\Omega_{LF-VF})]^{\mathrm{t}}\boldsymbol{D}_1 P_{eq}[\hat{\mathrm{J}}(\Omega_{VF-OF}) - \hat{\mathrm{J}}(\Omega_{LF-VF})]P_{eq}^{-1} \tag{2}$$

where $\hat{\mathrm{J}}(\Omega_{VF-OF})$ and $\hat{\mathrm{J}}(\Omega_{LF-VF})$ are the angular momentum operators for the probe and the protein, respectively.[34] Note that $\Omega_{LF-VF} = \Omega_{LF-M1F} + \Omega_{M1F-VF}$. (That is, Ω_{LF-VF} represents the combined effects of rotations by both sets of Euler angles on the right of this equation, where Ω_{M1F-VF} is time-independent.)

The Boltzmann distribution is $8\pi^2 P_{eq} = \exp[-U(\Omega_{VF-OF})/k_BT]/\langle\exp[-U(\Omega_{VF-OF})/k_BT]\rangle$, where $\langle\ldots\rangle$ means averaging over Ω_{VF-OF}. In general, the potential $U(\Omega_{VF-OF})$ is expanded in the full basis set of the Wigner rotation matrix elements. When only the $L = 2$ terms are preserved, one has[36,37,40]

$$u(\Omega_{VF-OF}) = \frac{U(\Omega_{VF-OF})}{k_BT} \approx -c_0^2 D_{0,0}^2(\Omega_{VF-OF}) - c_2^2[D_{0,2}^2(\Omega_{VF-OF}) + D_{0,-2}^2(\Omega_{VF-OF})] \tag{3}$$

The coefficient c_0^2 evaluates the strength of the POMF and c_2^2 its nonaxiality.

The local order parameters are defined as[36,37,40]

$$\langle D_{0m}^2(\Omega_{VF-OF})\rangle = [\int \mathrm{d}\Omega_{VF-OF} D_{0m}^2(\Omega_{VF-OF})\exp[-u(\Omega_{VF-OF})]] / [\int \mathrm{d}\Omega_{VF-OF}\exp[-u(\Omega_{VF-OF})]] \tag{4}$$

For at least 3-fold symmetry around the local director and at least 2-fold symmetry around the Z axis of the local ordering frame, only $S_0^2 \equiv \langle D_{00}^2(\Omega_{VF-OF})\rangle$ and $S_2^2 \equiv \langle D_{02}^2(\Omega_{VF-OF}) + D_{0,-2}^2(\Omega_{VF-OF})\rangle$ survive for $L = 2$.[57,58] The Saupe scheme order parameters relate to S_0^2 and S_2^2 as $S_{xx} = ((3/2)^{1/2}S_2^2 - S_0^2)/2$, $S_{yy} = -((3/2)^{1/2}S_2^2 + S_0^2)/2$, and $S_{zz} = S_0^2$.[57,58] In this study, we assume that 3-fold symmetry also prevails around the Z axis of the local ordering frame. In this case, the second term on the right of eq 3 is zero, and $S_2^2 = 0$ ($S_{xx} = S_{yy}$).

Equation 1 is solved to yield the SRLS time correlation functions that lead by Fourier transformation to the spectral densities, $j_{K,K'}(\omega) = \Sigma_i(c_{K,K',i}\tau_i)/(1 + \omega^2\tau_i^2)$.[36,37,40] In practice, a finite number of terms is sufficient for numerical convergence of the solution. The $j_{K,K'}(\omega)$ functions are assembled into the measurable spectral densities according to the local geometry (e.g., see Chapter 12 of ref 58). For N−H bond dynamics, the

dx.doi.org/10.1021/jp208767s |J. Phys. Chem. B 2012, 116, 886–894

relevant measurable spectral densities are $J^{DD}(\omega)$ for the $^{15}N-^{1}H$ dipolar interaction and $J^{CC}(\omega)$ for the ^{15}N CSA interaction. $J^{DD}(\omega)$ and $J^{CC}(\omega)$ are obtained from the $j_{K,K'}(\omega)$ functions by Wigner rotations based on Ω_{OF-DF} and Ω_{OF-CF}, respectively.

Cross-correlated spin relaxation, featuring $J^{XY}(\omega)$, is treated in complete analogy with autocorrelated spin relaxation.[37] $J^{DC}(\omega)$ is obtained from the $j_{K,K'}(\omega)$ functions by the Wigner rotation $R(\Omega_{OF-DF})$, followed by the Wigner rotation $R(\Omega_{DF-CF})$. The cross-correlation term is eliminated in the experiments used to acquire ^{15}N T_1, T_2 and $^{15}N-\{^{1}H\}$ NOE in proteins; this term is measured in separate experiments.

For rhombic local ordering and axial (e.g., dipolar) magnetic interaction, six distinct pairs, $K,K' = (0,0)$, $(1,1)$, $(2,2)$, $(0,2)$, $(-1,1)$, and $(-2,2)$, have to be considered. For axial local ordering, assumed in this study, only the components $K,K = (0,0)$, $(1,1)$, and $(2,2)$ have to be considered (reducing significantly the computational effort). In this case, the explicit expression for $J^{DD}(\omega)$ is

$$J^{DD}(\omega) = (d^2_{00}(\beta_{OF-DF}))^2 j_{00}(\omega) + 2(d^2_{10}(\beta_{OF-DF}))^2 j_{11}(\omega) + 2(d^2_{20}(\beta_{OF-DF})^2 j_{22}(\omega) \quad (5)$$

The expression for $J^{CC}(\omega)$ is analogous to eq 5, with β_{OF-DF} replaced by β_{OF-CF}. Alternatively, $J^{CC}(\omega)$ may be derived from $J^{DD}(\omega)$ by carrying out the Wigner rotation $R(\Omega_{DF-CF})$.

The autocorrelated ^{15}N relaxation parameters T_1, T_2 and $^{15}N-\{^{1}H\}$ *NOE* are calculated as a function of $J^{DD}(0)$, $J^{DD}(\omega_H)$, $J^{DD}(\omega_N)$, $J^{DD}(\omega_H - \omega_N)$, $J^{DD}(\omega_H + \omega_N)$, $J^{CC}(0)$, $J^{CC}(\omega_N)$, and the magnetic interactions, using standard expressions for NMR spin relaxation.[59−61] The cross-correlated relaxation rates associated with N−H bond dynamics, η_z and η_{xy},[62] feature the measurable spectral density, $J^{DC}(\omega)$, obtained as outlined above, and the $^{15}N-^{1}H$ dipolar/^{15}N CSA magnetic interaction cross-term.

Our most recent fitting scheme for SRLS allows separating the local ordering and the local diffusion frames. We call this software package C++OPPS (COupled Protein Probe Smoluchowski). It is available at the website http://www.chimica/unipd.it/licc/software.html, and described in detail in ref 37.

As pointed out above, the parameter combination appropriate for analyzing given experimental data is determined by requiring good correspondence between theory and experiment, internal consistency, and physical tenability of the results. For example, using six data points (^{15}N T_1, T_2 and $^{15}N-\{^{1}H\}$ *NOE* acquired at two magnetic fields), we found previously that allowing D_2, c^2_0, c^2_2, and β_{OF-DF} to vary is an appropriate scheme.[36,37,40] In this study, we introduce a different methodology. We allow $D_{2,\parallel}$, $D_{2,\perp}$, β_{OF-DF}, β_{M2F-OF}, and c^2_0 to vary, with the starting value of $D_{2,\perp}$ set equal to D_1, the starting value of β_{OF-DF} corresponding to the principal local ordering axis pointing along $C^{\alpha}_{i-1}-C^{\alpha}_{i}$, and the starting value of β_{M2F-OF} corresponding to the principal local diffusion axis pointing along the N−H bond.

2.2. Model-Free. The MF approach gives directly the measurable spectral density $J(\omega) = J^{DD}(\omega) = J^{CC}(\omega)$, made up of two Lorentzian terms that represent the global motion and a single (effective) local motion.[28,29] This simple form is based on the premise that these dynamic processes are statistically independent by virtue of being time-scale separated.[28] In addition, all the tensorial properties are simple: the global diffusion is isotropic, the local motion is isotropic, the local ordering is axial, and its principal axis is collinear with the principal axis of all the collinear (axial) magnetic tensors involved. Under these circumstances, the MF spectral density, $J(\omega) = j_{00}(\omega)$, is given by[28]

$$J(\omega) = S^2\tau_m/(1 + \tau_m{}^2\omega^2) + (1 - S^2)\tau_e{}'/1 + \tau_e{}'^2\omega^2) \quad (6)$$

The parameter τ_m is the correlation time for the global motion, and $\tau_e \ll \tau_m$ is the effective correlation time for the local motion. By virtue of $\tau_e \ll \tau_m$, one has $1/\tau_e{}' = 1/\tau_m + 1/\tau_e \sim 1/\tau_e$. S^2 is defined as the plateau value, $C^L(\infty)$, to which the local motional time correlation function, $C^L(t)$, converges at long times. Mathematically, $C^L(\infty)$ is given by $\Sigma_{m=0,\pm1,\pm2} |\langle Y_{2m}(\theta,\phi)\rangle\langle Y^*_{2m}(\theta,\phi)\rangle|$, where Y_{2m} are the spherical harmonics of Brink and Satchler.[63] The generalized order parameter is defined as $S \equiv (C^L(\infty))^{1/2}$.[28] S^2 is considered to represent the amplitude of the local motion. In the context of the physical definition of the order parameter[57,58] that enters the physical limit of MF,[54] this is appropriate when the POMT is axial and strong, and the local motion is so fast that its effect on the spin relaxation is completely averaged out.[34] On the basis of the theory of moments, τ_e is defined as the area of the exact time correlation function for internal motion (corresponding to a frozen protein[28]) divided by $(1 - S^2)$.

The extended MF (EMF) spectral density[30] features a fast local motion with effective correlation time, $\tau_f' = \tau_m\tau_f/(\tau_m + \tau_f) \approx \tau_f$, and squared order parameters, S^2_f, and a slow local motion with effective correlation time, $\tau_s' = \tau_m\tau_s/(\tau_m + \tau_s)$, and squared order parameter, S^2_s. All three dynamic modes, represented by τ_m, τ_f, and τ_s', are assumed to be decoupled from one another. In practice, τ_s' and τ_m are allowed to occur on the same time scale.

Model-free analytical time correlation functions, considered more general, have also been suggested. As pointed out above, their generality is substantiated through physically vague constructs.[56]

3. RESULTS AND DISCUSSION

3.1. MF Analysis. We start with a survey of the picture provided by previous MF analyses of ^{15}N spin relaxation from *E. coli* RNase H. In the first study, a data set comprising ^{15}N T_1, T_2 and $^{15}N-\{^{1}H\}$ *NOE* from 118 $^{15}N-H$ bonds, acquired at 11.7 T and 300 K, was analyzed.[11] In a later study,[17] 55, 10, 40, and 1 N−H bonds could be fit from a statistical point-of-view allowing S^2 (model 1), S^2 and τ_e (model 2), S^2 and R_{ex} (model 3), or S^2, τ_e, and R_{ex} (model 4) to vary. The data of 18 $^{15}N-H$ bonds required the reduced EMF model (where τ_f is set equal to zero), denoted model 5,[11] which describes dynamics that is more intricate. Local motional correlation times assuming values in the range of 0.83 to 4.5 ns have been ascribed to these N−H bonds, which reside mostly within loops. The correlation between the MF analysis and the structural context turned out to be limited. For example, ten N−H bonds from the loop α_C/α_D were analyzed, but only one required the reduced EMF model. Eleven N−H bonds of the C-terminal segment were analyzed: only four required the reduced EMF model, whereas the other seven could be analyzed with the simplest model 1.

^{15}N T_1, T_2 and $^{15}N-\{^{1}H\}$ *NOE* were also acquired in ref 17 at 285 and 310 K, and 11.7 T. The temperature-dependent data were analyzed with MF.[17] A characteristic temperature, T^*, of 2500 K (ref 64) was determined for the secondary structure elements from the temperature-dependence of S and a limiting form of the local ordering potential (given in general by the

Legendre polynomial of rank 2).[17] The parameter T^* is given by $c_0^2 \times T$ (K), where c_0^2 is the (unit-less) coefficient of the (axial) local potential. This yields $c_0^2 = 8.1$ at 300 K, which corresponds to $S^2 = 0.76$ (eqs 3 and 4). The MF analysis determined $\langle S^2 \rangle = 0.881$ for the secondary structure elements at 300 K; this yields $c_0^2 = 16.6$ (eqs 3 and 4). The difference between the corresponding squared order parameters (of smaller uncertainty in the large order parameter regime than the potential coefficients)[51] is 14%.

In ref 25, the variability of the ^{15}N CSA tensor was investigated. Single-field data from ninety-three relatively rigid N−H bonds free of R_{ex} contributions were used. We applied the MF program DYNAMICS[65] to these N−H bonds to find that 66 (43)% of the two-field data acquired at 11.7 and 14.1 T (14.1 and 18.8 T) lead to R_{ex} contributions on the order of 1 s^{-1} or greater. Only 38% of these contributions are common to both data sets; for 55%, R_{ex} at 14.1 T is smaller than R_{ex} at 11.7 T, contrary to the fast-exchange paradigm.

Clearly, many R_{ex} terms are artificial. One can prevent their appearance by virtually eliminating the local motion from the analysis and allowing instead the ^{15}N chemical shift anisotropy (CSA) tensor to vary.[66] When local motions are accounted for, the variations in the ^{15}N CSA tensor have been reported to be limited.[25,67]

Artificial R_{ex} terms can also be eliminated by allowing the global diffusion tensor to be nonspherically symmetric.[37,38,68] This feature of MF analyses, as applied to *E. coli* RNase HI, is discussed in ref 26. We address this matter in further detail below.

3.2. SRLS Analysis. *3.2.1. Global Diffusion.* Using the standard MF method based on experimental ^{15}N T_1 and T_2 data, the global diffusion tensor was determined to be axially symmetric, with $D_{1,iso} = (1.72 \pm 0.01) \times 10^7$ s^{-1} and $D_{1,\parallel}/D_{1,\perp} = 1.23$.[26] Using these global motional parameters and typical local motional parameters obtained with SRLS/C++OPPS analysis, we calculated ^{15}N T_1, T_2 and ^{15}N−{^{1}H} *NOE* for angles, β_{M1F-VF}, of 0° and 90° between the principal axis of the global diffusion tensor, Z_{M1F}, and the equilibrium orientation of the N−H bond, VF. The percent differences between corresponding relaxation parameters, which evaluate the maximum effect a $\boldsymbol{D_1}$ axiality of 1.23 has on the analysis, are −2.9 to −3.6 for ^{15}N T_1, 3.5 to 4.2 for ^{15}N T_2, and 0.2 to 0.3 for the ^{15}N−{^{1}H} *NOE*, for magnetic fields of 14.1 and 18.8 T. For most N−H bonds, the effect is smaller, lying typically within the uncertainty limits (see below) of the best-fit SRLS parameters.

On the basis of these findings we took the global diffusion tensor to be isotropic, as done in refs 11, 17, and 25. Note that MF overestimates the effect of global diffusion axiality (or asymmetry) on the analysis because unaccounted for factors associated with the restricted local motion are often absorbed by the $\boldsymbol{D_1}$ tensor.[36−38,40]

With D_1 set equal to 1.8×10^7 s^{-1},[17] we proceed analyzing the experimental ^{15}N relaxation data of RNase H acquired at 14.1 and 18.8 T and 300 K as follows. In all of the scenarios discussed below, the χ^2/df (where df denotes the number of degrees of freedom) values are mostly below the 0.05 critical values (5.99, 7.81, 9.49, and 11.1 for df = 2, 3, 4, and 5).

Allowing to vary (1) c_0^2 and fixing D_2 at, say, 10^{11} s^{-1}; (2) c_0^2 and D_2; (3) S^2 and R_{ex}; and (4) S^2, D_2, and R_{ex}, are scenarios that may be associated formally with models 1, 2, 3, and 4 in MF. These SRLS schemes reproduce the general trends in the corresponding best-fit MF parameters. Significant quantitative differences stem from the fact that the actual time correlation function is not biexponential.[36,40] Furthermore, mode-coupling is a small effect for rigid MF bonds, but is likely to affect the analysis of N−H bonds residing within loops. Finally, SRLS accounts for the tilt angle between the ^{15}N−^{1}H dipolar and (axial) ^{15}N CSA tensors, while in MF, this angle is implicitly zero.[36]

We found that the D_2 profile obtained with these simple models is very problematic (note that τ_e, its formal analogue, can often not be determined in MF analyses). A significant part of the inconsistencies outlined in section 3.1. are preserved. Importantly, the asymmetry of the local spatial restrictions is not borne out. As shown above, most R_{ex} terms do not represent physical conformational exchange. We do not accept the simple models described above, set R_{ex} equal to zero, and proceed by enhancing the tensorial properties of the local diffusion and local ordering. A straightforward enhancement is to allow the principal axis of the local ordering tensor to be tilted from the principal axis of the ^{15}N−^{1}H dipolar tensor, i.e., from the N−H bond; the respective angle, β_{OF-DF}, is denoted β_D for brevity.

The SRLS spectral density, $J^{DD}(\omega)$, that corresponds to $\beta_{OF-DF} \neq 0$ is given by eq 5. One may consider model 5 in MF (where $J(\omega) = J^{DD}(\omega) = J^{CC}(\omega)$) to be formally a truncated form of eq 5 where the second and third terms have been omitted, and $j_{00}(\omega)$ has been replaced by eq 6. The coefficients of the terms in a physical spectral density have to sum up to 1. Mere elimination of terms from such a function implies inaccurate best-fit parameters that absorb the effect of the omitted terms; this scenario represents force-fitting.[36,40] Simplifications should be made by designing the appropriate Markov operator. Moreover, the trigonometric factor $(d_{00}^2\ (\beta_{OF-DF}))^2$ in eq 5 is considered in MF to represent the square of an order parameter, S_f^2. Thus, model 5 in MF is based on a problematic spectral density. Note that the EMF formula from which model 5 is derived is given within a good approximation by eq B6 of ref 55, which is only valid in the large time-scale separation between the global and local motions, while in MF analyses, τ_s' is typically on the same time scale as τ_m.

The results of the SRLS calculations that are formally analogous to MF model 5 are shown in Figure 3. The parameters c_0^2, D_2, and β_D corresponding formally to the MF parameters S^2, τ_s', and S_f^2, respectively,[35,36,40] were allowed to vary in these calculations. Approximately 10% of the results obtained have been eliminated as emerging from force-fitted experimental data. Substantial variations are noticeable in c_0^2 within all the helices (Figure 3a) and in S_0^2 within the helices α_C and α_E (Figure 3b). Such structural diversity within the helices of *E. coli* RNase is not supported by its 3D structure.[12−14] The local motion in the α_A helix in slower than in the loops. *E. coli* RNase was studied extensively with MF.[11,15,17] Slow segmental motion of the α_A helix was not reported either by these studies or by studies based on other physical methods. Such motion should have been detected at least qualitatively. There are significant differences between the results obtained using combined 11.7 and 14.1 T, 14.1 and 18.8 T, and 11.7, 14.1, and 18.8 T experimental data. It may be concluded that merely allowing the axial local ordering tensor to be tilted from the ^{15}N−^{1}H dipolar tensor does not materialize properly the actual asymmetry of the local spatial restrictions. We do not accept the model underlying the results shown in Figure 3, although statistically the experimental data are fit properly.

Some of the c_0^2 values in Figure 3 appear to be unduly large. However, they are tenable physically. In the strong ordering limit, the functional dependence of $(S_0^2)^2$ on c_0^2 approaches a plateau value (e.g., see Figure 2 of ref 35). Therefore, small changes in

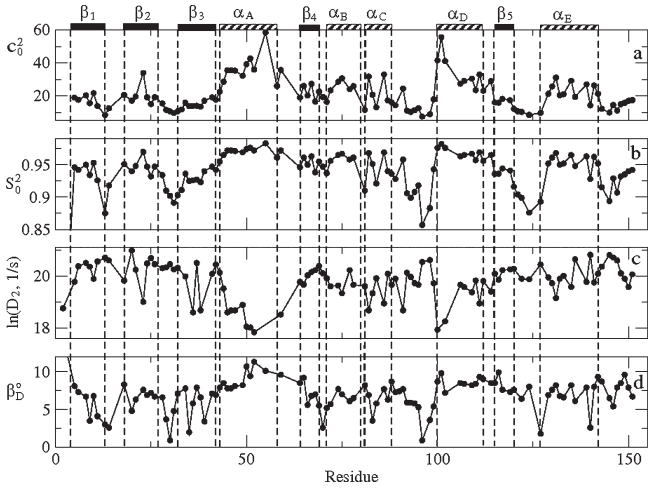

Figure 3. Best-fit value of c_0^2, the coefficient of the axial local potential (a); S_0^2, the order parameter defined in terms of this potential (b); ln(D_2, 1/s), where D_2 is the local motional rate (c); and β_D, the tilt angle of the principal axis of the local ordering tensor, ***S***, from the N−H bond (d). These results were obtained by allowing c_0^2, D_2, and β_D to vary. The errors are estimated at 2% for all the parameters. In the calculations shown in this figure and all of the subsequent figures we used an ^{15}N CSA value of −172 ppm, a bond length r_{NH} = 1.02 Å, and a −17° tilt angle between the ^{15}N−^{1}H dipolar and ^{15}N CSA tensor frames.[37]

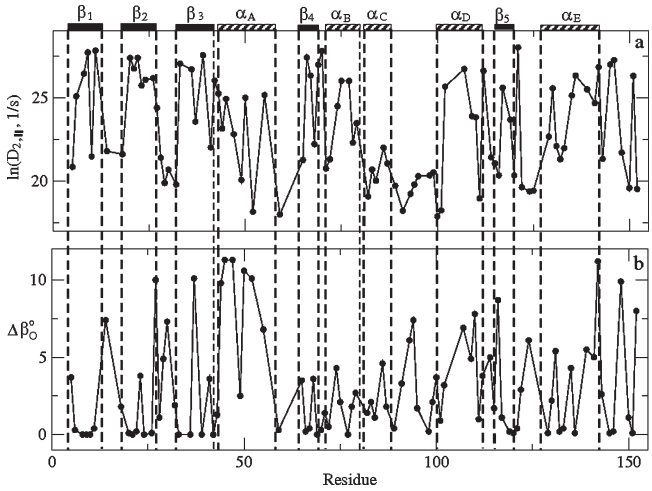

Figure 4. Best-fit value of ln($D_{2,\parallel}$, 1/s) (a) and $\Delta\beta_O$ (b) obtained by allowing c_0^2, $D_{2,\parallel}$, β_D and β_O to vary as outlined in the text, and fixing $D_{2,\perp} = D_1$. The errors are estimated at 2% for c_0^2 (not shown), ln($D_{2,\parallel}$, 1/s), $\Delta\beta_D$ (not shown), and $\Delta\beta_O$.

(S_0^2)^2 correspond to large changes in c_0^2. For example, c_0^2 = 20 (in units of k_BT) corresponds to (S_0^2)^2 = 0.9. Values of c_0^2 larger than 20 correspond to (S_0^2)^2 values only somewhat larger than 0.9, which are realistic. Thus, the principal value of the local ordering tensor, S_0^2, rather than the coefficient of the local potential, c_0^2 (in terms of which S_0^2 is defined), is to be considered for an accurate estimate of the strength of the local restrictions at relatively rigid N−H sites in proteins. In this context, it should be pointed out that in S_0^2 (or c_0^2) and β_D are conceptually different quantities, related to the principal value and orientation of the local ordering tensor, respectively. Only when the local motion is so fast that it no longer affects the spin relaxation directly, and the local ordering potential is axially symmetric and very strong, may geometric features be associated with the mean square fluctuation amplitude of all the internal motions.[34]

We proceed by taking the D_2 tensor to be axially symmetric, i.e., allowing both $D_{2,\parallel}$ and $D_{2,\perp}$ (instead of only D_2) to vary. This extension led in quite a few cases to high χ^2 or negative local motional rates, most likely because the orientations of the ***S*** and $\boldsymbol{D_2}$ tensors are not accounted for properly. We proceed by improving these geometric features.

As pointed out above, there is substantial evidence that the main local ordering axis at N−H sites in proteins is associated with the $C_{i-1}^{\alpha}-C_i^{\alpha}$ axis.[36−38,40−43,46−50] On the basis of this, we take the starting value of β_D as −101.3°, the established angle between the N−H bond and the $C_{i-1}^{\alpha}-C_i^{\alpha}$ axis,[42] and allow β_D to vary. We show below the difference, $\Delta\beta_D$, between the best-fit value of β_D and −101.3°. The angle $\Delta\beta_D$ represents the deviation of Z_{OF} from the $C_{i-1}^{\alpha}-C_i^{\alpha}$ axis; the order parameter S_0^2 represents the strength of the local ordering around Z_{OF}.

A detailed residual dipolar coupling study of the third IgG-binding domain of protein G (GB3) reported on out-of-plane N−H motions.[69] These dynamic processes, N−H bond vector fluctuations reported by MD studies,[70] and nitrogen pyramidalization[71] are all centered at the N−H bond. On the basis of this evidence, we take the starting value of the principal axis of the local diffusion tensor to be parallel to the N−H bond (substantiated within the scope of the SRLS frame scheme (Figure 2) by setting $\beta_{M2F-OF} \equiv \beta_O$ equal to −101.3° and allowing β_O to vary). We show below the difference between the best-fit value of β_O and −101.3°. The angle $\Delta\beta_O$ represents the deviation of Z_{M2F} from the N−H bond; $D_{2,\parallel}$ and $D_{2,\perp}$ are the local motional rates around Z_{M2F} and $X_{M2F} = Y_{M2F}$, respectively.

For small values of $\Delta\beta_O$, as found herein, $D_{2,\parallel}$ represents N−H bond vector fluctuations around the equilibrium N−H orientation. We found that starting values of $D_{2,\parallel}$ in the 1.0 × 10^9−5.0 × 10^{10} s^{-1} range, and c_0^2 in the 10−15 range (which represent, as expected, relatively fast N−H fluctuations in the presence of relatively strong local ordering) lead virtually to the same minimum. For small values of $\Delta\beta_O$, the parameter $D_{2,\perp}$ monitors motions around an axis nearly perpendicular to the N−H bond, i.e., nearly parallel to the $C_{i-1}^{\alpha}-C_i^{\alpha}$ axis. It is reasonable to interpret $D_{2,\perp}$ as representing the rate of global diffusion of the protein, which at 300 K is given by D_1 = 1.8 × 10^7 s^{-1}. This scheme was used in previous work.[37,72]

We show in Figure 4a,b best-fit values of ln($D_{2,\parallel}$, 1/s) and $\Delta\beta_O$ obtained by allowing c_0^2, $D_{2,\parallel}$, β_D, and β_O to vary (with starting values of 10 for c_0^2, 1.8 × 10^9 s^{-1} for $D_{2,\parallel}$, and −101.3° for the two angles), and presetting $D_{2,\perp}$ = 1.8 × 10^7 s^{-1}. In Figure 5c,d, we show the analogous results obtained by also allowing $D_{2,\perp}$ to vary starting from D_1 = 1.8 × 10^7 s^{-1}. Although ln($D_{2,\perp}$, 1/s) varies only within 5% of ln(D_1, 1/s), it is obvious that Figure 5c,d agrees with the structural context significantly better than Figure 4a,b. It is our experience[36,40,51−53] that parameters that we would like to fix at their established values (e.g., fix β_D at 101.3°, the standard angle between the N−H bond and the $C_{i-1}^{\alpha}-C_i^{\alpha}$ axis) have to be allowed to vary starting from these values to render the fitting process effective. In support of these assignments, the best-fit values of these parameters are in most cases quite close to their respective starting values.

We also checked the dependence of the results on the data set used. The results are generally reproducible within an error margin of 10% when various combined two-field data sets, or the three-field data set, are used. To our knowledge, such level of internal consistency is not achievable with standard MF analyses.

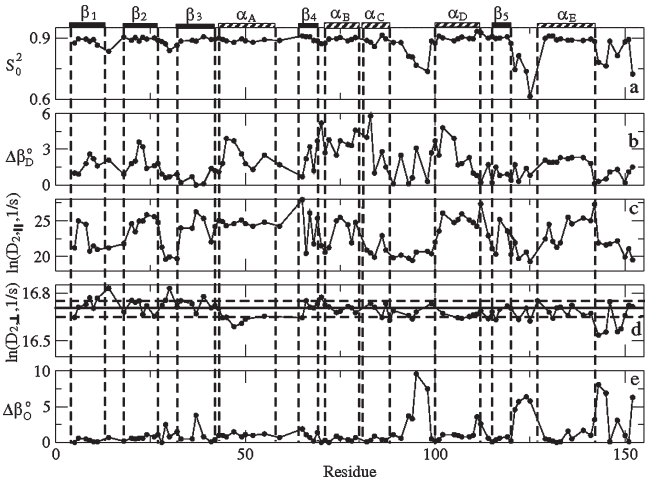

Figure 5. Best-fit value of S_0^2 (a), $\Delta\beta_D$ (b), $\ln(D_{2,\parallel}, 1/s)$ (c), $\ln(D_{2,\perp}, 1/s)$ (d), and $\Delta\beta_O$ (e) obtained by allowing c_0^2, $D_{2,\parallel}$, $D_{2,\perp}$, β_D, and β_O to vary as outlined in the text. The errors are estimated at 2% for S_0^2, $\Delta\beta_D$, $\ln(D_{2,\parallel}, 1/s)$, and $\Delta\beta_O$ and 5% for $\ln(D_{2,\perp}, 1/s)$.

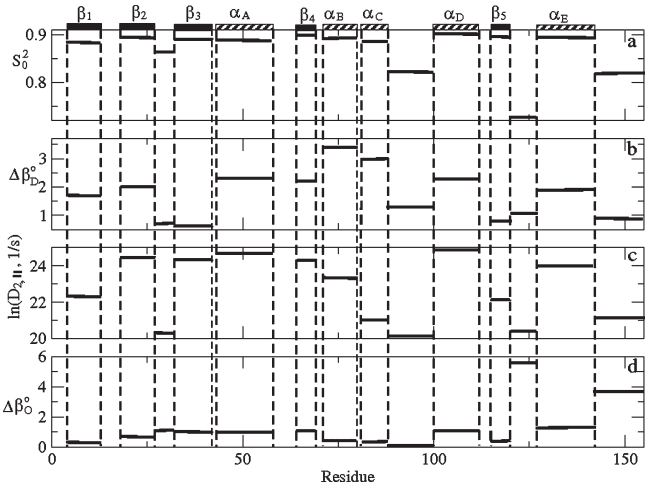

Figure 6. Average values for the various secondary structure elements and loops calculated from Figure 5. The errors are estimated at 2% for S_0^2, $\Delta\beta_D$, $\ln(D_{2,\parallel}, 1/s)$, and $\Delta\beta_O$ and 5% for $\ln(D_{2,\perp}, 1/s)$.

The errors in the best-fit parameters have been evaluated based on the uncertainties in the results implied by varying the starting values of the variables.[71] This consideration led to an estimate of 2% error for all of the parameters except for $\ln(D_{2,\perp}, 1/s)$. In this case, we consider 5% as a realistic estimate, based on the requirement that $\ln(D_{2,\perp}, 1/s) \geq \ln(D_1, 1/s)$, which is fulfilled within this uncertainty limit (except for several cases within the α_A helix and the C-terminal segment).

With the scheme outlined above, the results agree with the structural context, their uncertainties are acceptable, and the inconsistencies characteristic of the simpler models have been largely eliminated. We adopt the model described above as appropriate for deriving new information. The best-fit values of S_0^2, $\Delta\beta_D$, $\ln(D_{2,\parallel}, 1/s)$, $\ln(D_{2,\perp}, 1/s)$, and $\Delta\beta_O$ are shown in Figure 5.

The profile of the local order parameter, S_0^2 (Figure 5a), indicates that, in general, the loops exhibit lower local ordering than the secondary structure elements. The loops α_C/α_D and β_5/α_E exhibit significantly lower local ordering. The average S_0^2 value for the secondary structure elements is 0.89 (Figure 6a). This corresponds to $(S_0^2)^2 = 0.79$, to be compared with the MF value of 0.881 for $\langle S^2 \rangle$.[17] For details, one has to examine carefully Figures 5a and 6a.

The deviation of the principal axis of the local ordering tensor from the $C_{i-1}^{\alpha}-C_i^{\alpha}$ axis, $\Delta\beta_D$, does not exceed 6° (Figure 5b). In the α_E helix, it assumes a nearly uniform value of 2°. The smallest (largest) deviation from the $C_{i-1}^{\alpha}-C_i^{\alpha}$ axis occurs in the β_3 strand (α_B helix) (Figure 6b). The alternations within the β_3 and β_4 strands, the α_B helix and the α_C/α_D loop, and the irregular pattern within the α_A helix require further investigation.

As expected, within the secondary structure elements the N−H bond vector fluctuations represented by $D_{2,\parallel}$ are fast. We illustrate this property in Figure 5c as $\ln(D_{2,\parallel}, 1/s)$. The variations among the secondary structure motifs are significant. The correlation time, $\tau_{\parallel} = 1/(6D_{2,\parallel})$, extends from 3 to 125 ps. Several N−H bonds within the α_C helix, and the β_1 and β_5 strands exhibit relatively slow fluctuations. Average values for the various α-helices and β-strands are depicted in Figure 6c. Substantially slower N−H bond vector fluctuations are detected for the loops. The average values for the α_C/α_D (β_5/α_E) loop is 344 (208) ps (Figure 6c). The C-terminal segment is associated with an average correlation time of 125 ps.

The perpendicular component of the local diffusion tensor, $\ln(D_{2,\perp}, 1/s)$, is shown in Figure 5d. The full line represents $\ln(D_1, 1/s)$, and the dashed lines delineate the uncertainty limit of 5%. It can be seen that $\ln(D_{2,\perp}, 1/s)$ is in most cases virtually the same as $\ln(D_1, 1/s)$. This is consistent with the equilibrium orientation of the N−H bond being fixed in the protein backbone, with the only local motional mode experienced being N−H fluctuations. One might ascribe tentatively $D_{2,\perp}$ rates somewhat faster than D_1 to the loops β_1/β_2 and β_2/β_3. This is consistent with localized ns motion of the protein backbone, taking place in addition to the collective rocking motions occurring on the 100 ns time scale, detected with solid-state NMR.[73]

The best-fit values of the $\Delta\beta_O$ angle are shown in Figure 5e. The deviations of the principal local diffusion axis from the N−H bond are in general below 2° for the secondary structure elements and below 10° for the loops α_C/α_D and β_5/α_E and the C−terminal segment. Although depicted in Figure 6d, the other loops are characterized so scarcely that we refrain from discussing them.

Figure 6 may be used to single out outstanding features of given structural elements. The α_C helix exhibits an average $D_{2,\parallel}$ rate characteristic of loops. The β_3 and β_5 strands exhibit very small average $\Delta\beta_D$ angles. These features require further investigation. The α_C/α_D loop has on average relatively weak local ordering, relatively slow local motion, and a relatively large $\Delta\beta_O$ angle as compared to the other loops. The β_5/α_E loop exhibits on average very weak local ordering and a relatively large $\Delta\beta_O$ angle as compared to the other loops. Together with the β_1/β_2 loop, these two loops have been suggested to participate in substrate binding. It is of interest to investigate the relationship between their dynamic structure and their function.

It is of interest to compare representative SRLS and MF results obtained for N−H bonds residing within loops, which experience intricate dynamics. We select as an example the N−H bonds of residues Ala 125, Gly 126, and His 127 of the β_5/α_E loop, analyzed in MF with model 5. The average SRLS S_0^2 (MF S) value is 0.70 (0.84). The average SRLS $\tau_{iso} = 1/(4D_{2,\perp} + 2D_{2,\parallel})$ (τ_s' MF)

value is 0.597 (1.09) ns. The angles $\Delta\beta_D$ and $\Delta\beta_O$ are nearly zero in SRLS; they are 13.1° ($S_f^2 = (1.5\cos^2\Delta\beta_D - 0.5)^2 = 0.836$) and 88.1° (101.3 − 13.2)° in MF. Clearly, the formally analogous parameters differ substantially in magnitude. Importantly, they have different meaning in the context of different geometric settings. The fact that the local motion is slower within loops as compared with secondary structure elements is borne out in SRLS by $D_{2,\parallel}$ within the scope of the same model. In MF, one has to resort to model 5 for loops and to models 1−4 for secondary structure elements.[11,17,26]

The tensorial description presented in this work within the scope of SRLS is the standard description of magnetic resonance spin relaxation. RNase is a typical relatively rigid protein; so are hemoglobin and carbon-monoxy hemoglobin.[72] Even for these proteins, a tensorial description (rather than the simple MF description), which accounts for general features of tensor symmetry and local geometry, is required. Within its scope, it has been possible to account in a physically sound manner for N−H bond vector fluctuations represented by $D_{2,\parallel}$ and slow backbone motions represented by $D_{2,\perp}$. So far, we considered diffusive local motion. SRLS allows for other types of local motion (e.g., jumps over energy barriers) by implementing local potentials of appropriate form (e.g., see Figure 4 of ref 33).

4. CONCLUSIONS

A useful SRLS-based method for analyzing ^{15}N spin relaxation in proteins has to feature the important asymmetry of the local spatial restrictions on the local motion of the N−H bond and be efficient computationally. SRLS describes the local restrictions in terms of a second-rank ordering tensor and the local motion in terms of a second-rank diffusion tensor. When these tensors are taken axial but their principal axes systems are tilted, they describe inherently an asymmetric setting. On the basis of this rationale, we developed a generally applicable methodology that reaches the objectives stated above and provides an insightful tensorial description of N−H bond structural dynamics.

The local ordering is found to be relatively strong within secondary structure elements ($\langle S_0^2\rangle = 0.89$) and weaker within loops ($\langle S_0^2\rangle = 0.84$). There are significant differences among the various structural motifs. The principal local ordering axis is nearly parallel to the $C_{i-1}^{\alpha}-C_i^{\alpha}$ axis. The perpendicular component of the local diffusion tensor is nearly the same as the rate of global tumbling. The parallel component of the local diffusion tensor represents N−H bond vector fluctuations centered within a good approximation around the equilibrium N−H orientation. They occur with average correlation times of 3−125 ps for secondary structure elements, 125−344 for loops, and 125 ps for the C-terminal segment, with substantial variations among the various structural motifs.

Prospects include combining SRLS with molecular dynamics to correlate the mesoscopic parameters with atomistic properties.

AUTHOR INFORMATION

Corresponding Author

*Phone: 972-3-531-8049. Fax: 972-3-738-4058. E-mail: meirove@biu.ac.il.

ACKNOWLEDGMENT

We thank Professor Arthur G. Palmer of Columbia University for providing the ^{15}N relaxation parameters from RNase H used in this study that have not been published in ref 25. This work was supported by the Israel Science Foundation (Grant No. 347/07 to E.M.), the Binational Science Foundation (Grant No. 2006050 to E.M. and J.H.F.), the German-Israeli Science Foundation for Scientific Research and Development (Grant No. 928-190.0/2006 to E.M. and Christian Griesinger of Max Planck Institute, Göttingen, Germany), and the Damadian Center for Magnetic Resonance at Bar-Ilan University, Israel. A.P. acknowledges support provided by the Ministero dell'Istruzione, Università e Ricerca (MIUR), grant 2008J9RNB3 PRIN 2008 TIME, and by the University of Padova, grant STPD08RCX5 "Progetto Strategico" HELIOS.

REFERENCES

(1) Stein, H.; Hausen, P. *Science* **1969**, *166*, 393.
(2) Crouch, R. J.; Dirksen, M.-L. *Nuclease*; Linn, S. M., Roberts, R. J., Eds.; Cold Spring Harbor Laboratory Press: Cold Spring Harbor, NY, 1982; pp 211−241.
(3) Crouch, R. J. *New Biol.* **1990**, *2*, 771.
(4) Berkower, I.; Leis, J.; Hurvitz, J. *J. Biol. Chem.* **1973**, *248*, 5914.
(5) Itoh, T.; Tomizawa, J. *Proc. Natl. Acad. Sci. U.S.A.* **1980**, *77*, 2450.
(6) Tomizawa, J. *Cell* **1984**, *38*, 861.
(7) Dasgupta, S.; Masukata, H.; Tomizawa, J. *Cell* **1987**, *51*, 1113.
(8) deMassy, B.; Fayet, O.; Kogoma, T. *J. Mol. Biol.* **1984**, *178*, 227.
(9) Horiuchi, T.; Maki, H.; Sekiguchi, M. *Mol. Gen. Genet.* **1984**, *195*, 17.
(10) Kitani, T.; Yoda, K.; Qgawa, T.; Okazaki, T. *J. Mol. Biol.* **1985**, *184*, 45.
(11) Mandel, A. M.; Akke, M.; Palmer, A. G., III. *J. Mol. Biol.* **1995**, *246*, 144.
(12) Yang., W.; Hendrickson, W. A.; Crouch, R. J. *Science* **1990**, *249*, 1398.
(13) Katayangi, K.; Miyagawa, M.; Matsushima, M.; Ishikawa, S.; Kanaya, S.; Ikehara, M.; Matsuzaki, T.; Morikawa, K. *Nature* **1990**, *347*, 306.
(14) Katayangi, K.; Miyagawa, M.; Matsushima, M.; Ishikawa, S.; Kanaya, S.; Nakamura, H.; Ikehara, M.; Matsuzaki, T.; Morikawa, K. *J. Mol. Biol.* **1992**, *223*, 1029.
(15) Yamazaki, T.; Yoshida, M.; Nagayama, K. *Biochemistry* **1993**, *32*, 5656.
(16) Kraulis, P. J. *J. Appl. Crystallogr.* **1991**, *24*, 946.
(17) Mandel, A. M.; Akke, M.; Palmer, A. G., III. *Biochemistry* **1996**, *35*, 16009.
(18) Yamazaki, T.; Yoshida, M.; Kanaya, S.; Nakamura, H.; Nagayama, K. *Biochemistry* **1991**, *30*, 6036.
(19) Nakamura, H.; Oda, Y.; Iwai, S.; Inoue, H.; Ohtsuka, E.; Kanaya, S.; Kimura, S.; Katsuda, C.; Katayanagi, K.; Morikawa, K.; Miyashiro, H.; Ikehara, M. *Proc. Natl. Acad. Sci. U.S.A.* **1991**, *88*, 11535.
(20) Oda, Y.; Iwai, S.; Ohtsuka, E.; Ishikawa, M.; Ikehara, M.; Nakamura, H. *Nucleic Acids Res.* **1993**, *21*, 4690.
(21) Nagayama, K.; Yamazaki, T.; Yoshida, M.; Kahaya, S.; Nakamura, H. *J. Biochem.* **1990**, *108*, 149.
(22) Oda, Y.; Nakamura, H.; Kanaya, S.; Ikehara, M. *J. Biomol. NMR* **1991**, *1*, 247.
(23) Oda, Y.; Nakamura, H.; Yamazaki, T.; Nagayama, K.; Yoshida, M.; Kanaya, S.; Ikehara, M. *J. Biomol. NMR* **1992**, *2*, 137.
(24) Oda, Y.; Yamazaki, T.; Nagayama, K.; Kanaya, S.; Kuroda, Y.; Nakamura, H. *Biochemsitry* **1994**, *33*, 5275.
(25) Kroenke, C. D.; Rance, M.; Palmer, A. G., III. *J. Am. Chem. Soc.* **1999**, *121*, 10119.
(26) Butterwick, J. A.; Loria, J. P.; Astrof, N. S.; Kroenke, C. D.; Cole, R.; Rance, M.; Palmer, A. G., III. *J. Mol. Biol.* **2004**, *339*, 855.
(27) Butterwick, J. A; Palmer, A. G., III. *Protein Sci.* **2006**, *15*, 2697.
(28) Lipari, G.; Szabo, A. *J. Am. Chem. Soc.* **1982**, *104*, 4546.
(29) Lipari, G.; Szabo, A. *J. Am. Chem. Soc.* **1982**, *104*, 4559.
(30) Clore, G. M.; Szabo, A.; Bax, A.; Kay, L. E.; Driscoll, P. C.; Gronenborn, A. M. *J. Am. Chem. Soc.* **1990**, *112*, 4989.

(31) Baber, J. L.; Szabo, A.; Tjandra, N. *J. Am. Chem. Soc.* **2001**, *123*, 3953.
(32) Polimeno, A.; Freed, J. H. *Adv. Chem. Phys.* **1993**, *83*, 89.
(33) Polimeno, A.; Freed, J. H. *J. Phys. Chem.* **1995**, *99*, 10995.
(34) Liang, Z.; Freed, J. H. *J. Phys. Chem. B* **1999**, *103*, 6384.
(35) Tugarinov, V.; Liang, Z.; Shapiro, Y. E.; Freed, J. H.; Meirovitch, E. *J. Am. Chem. Soc.* **2001**, *123*, 3055.
(36) Meirovitch, E.; Shapiro, Y. E.; Polimeno, A.; Freed, J. H. *J. Phys. Chem. A* **2006**, *110*, 8366.
(37) Zerbetto, M.; Polimeno, A.; Meirovitch, E. *J. Phys. Chem. B* **2009**, *113*, 13613.
(38) Meirovitch, E.; Shapiro, Y. E.; Tugarinov, V.; Liang, Z.; Freed, J. H. *J. Phys. Chem. B* **2003**, *107*, 9883.
(39) Meirovitch, E.; Shapiro, Y. E.; Liang, Z.; Freed, J. H. *J.Phys. Chem. B* **2003**, *107*, 9898.
(40) Meirovitch, E.; Shapiro, Y. E.; Polimeno, A.; Freed, J. H. *Prog. Nucl. Magn. Reson. Spectrosc.* **2010**, *56*, 360.
(41) Bremi, T.; Brüschweiler, R. *J. Am. Chem. Soc.* **1997**, *119*, 6672.
(42) Lienin, S. F.; Bremi, T.; Brutscher, B.; Bruschweiler, R.; Ernst, R. R. *J. Am. Chem. Soc.* **1998**, *120*, 9870.
(43) Fadel, A. R.; Jin, D. Q.; Montelione, G. T.; Levy, R. M. *J. Biomol. NMR* **1995**, *6*, 221.
(44) Clore, G. M.; Schwieters, C. D. *Biochemistry* **2004**, *43*, 10678.
(45) Buck., M.; Karplus, M. *J. Am. Chem. Soc.* **1999**, *121*, 9645.
(46) Tugarinov, V.; Shapiro, Y. E.; Liang, Z.; Freed, J. H.; Meirovitch, E. *J. Mol. Biol.* **2002**, *315*, 171.
(47) Shapiro, Y. E.; Kahana, E.; Tugarinov, V.; Liang, Z.; Freed, J. H.; Meirovitch, E. *Biochemistry* **2002**, *41*, 6271.
(48) Shapiro, Y. E.; Meirovitch, E. *J. Phys. Chem. B* **2006**, *110*, 11519.
(49) Shapiro, Y. E.; Kahana, E.; Meirovitch, E. *J. Phys. Chem. B* **2009**, *113*, 12050.
(50) Zerbetto, M.; Buck, M.; Meirovitch, E.; Polimeno, A. *J. Phys. Chem. B* **2011**, *115*, 376.
(51) Meirovitch, E.; Polimeno, A.; Freed, J. H. *J. Phys. Chem. B* **2006**, *110*, 20615.
(52) Meirovitch, E.; Shapiro, Y. E.; Polimeno, A.; Freed, J. H. *J. Phys. Chem. B* **2007**, *111*, 12865.
(53) Shapiro, Y. E.; Polimeno, A.; Freed, J. H.; Meirovitch, E. *J. Phys. Chem. B* **2011**, *115*, 354.
(54) Freed, J. H. *J. Chem. Phys.* **1977**, *66*, 4183.
(55) Lin, W. J.; Freed, J. H. *J. Phys. Chem.* **1979**, *83*, 379.
(56) Halle, B. *J. Chem. Phys.* **2009**, *131*, 224507.
(57) *NMR of Liquid Crystals*; Emsley, J. W., Ed.; Riedel: Dordrecht, The Netherlands, 1983.
(58) *The Molecular Dynamics of Liquid Crystals*; Luckhurst, G. R., Veracini, C. A., Eds.; Kluwer Academic Publishers: The Netherlands, 1994.
(59) Peng, J. W.; Wagner, G. In *Methods in Enzymology*; James, T. L., Oppenheimer, N. J., Eds.; Academic Press: New York, 1994; Vol. 239, pp 563−595.
(60) Abragam, A. *Principles of Nuclear Magnetism*; Oxford University Press (Clarendon): London, U.K., 1961.
(61) Cavanagh, J.; Fairbrother, W. J.; Palmer, A. G., III; Skelton, N. J. *Protein NMR Spectroscopy: Principles and Applcation*; Academic Press: San Diego, CA, 1996.
(62) Kroenke, C. D.; Loria, J. P.; Lee, L. K.; Rance., M.; Palmer, A. G., III. *J. Am. Chem. Soc.* **1998**, *120*, 7905.
(63) Brink, D. M.; Satchler, G. R. *Angular Momentum*; Clarendon Press: Oxford, U.K., 1968.
(64) Seewald, M. J.; Pichumani, K.; Stowell, C.; Tibbals, B. V.; Regan, L.; Stone, M. J. *Protein Sci.* **2000**, *9*, 1177.
(65) Fushman, D.; Cahill, S.; Cowburn, D. *J. Mol. Biol.* **1997**, *266*, 173.
(66) Hall, J. B.; Fushman, D. *J. Am. Chem. Soc.* **2006**, *128*, 7855.
(67) Damberg, P.; Jarvet, J.; Gräslund, A. *J. Am. Chem. Soc.* **2005**, *127*, 1995.
(68) Osborne, M. J.; Wright, P. E. *J. Biomol. NMR* **2001**, *19*, 209.
(69) Ulmer, T. S.; Ramirez, B. E.; Delaglio, F.; Bax., A. *J. Am. Chem. Soc.* **2003**, *125*, 9179.
(70) Case, D. A. *Acc. Chem. Res.* **2002**, *35*, 325.
(71) Mannfors, B. E.; Mirkin, N. G.; Palmo, K.; Krimm, S. *J. Phys. Chem. A* **2003**, *107*, 1825.
(72) Meirovitch, E.; Zerbetto, M.; Polimeno, A.; Freed, J. H. *J. Phys. Chem. B* **2011**, *115*, 143.
(73) Lewandowski, J. R.; Sein, J.; Blackledge, M.; Emsley, L. *J. Am. Chem. Soc.* **2010**, *132*, 1246.